Numerical modelling of blast-induced crack propagation in pre-fractured rock

Conference Paper

Author(s):
Liu, Huandui; Wang, Guibin; Lei, Qinghua ; Zhao, Xingguang

Numerical modelling of blast-induced crack propagation in pre-fractured rock

Huandui Liu[1], Guibin Wang[1], Qinghua Lei[1,2], Xingguang Zhao[3]

[1]State Key Laboratory of Geomechanics and Geotechnical Engineering, Institute of Rock and Soil Mechanics, Chinese Academy of Sciences, Wuhan, 430071, China;

[2]Chair of Engineering Geology, Department of Earth Sciences, ETH Zürich, Zürich, 8050, Switzerland

[3] Beijing Research Institute of Uranium Geology, CNNC, Beijing 100029, China

Correspondence should be addressed to Guibin Wang; gbwang@whrsm.ac.cn

Abstract. This paper presents a series of numerical simulations to investigate blast-induced crack propagation in rock specimens embedded with a pre-existing fracture. The simulation is conducted using the particle-based discrete element method, which can effectively capture many important geomechanical processes such as solid vibration, crack growth and fracture sliding. Particles are assembled based on the grain size distribution of Beishan granite using a Voronoi tessellation algorithm, with the parameters of particle contacts calibrated against to the laboratory testing results. The pre-existing fracture is represented using the model of smooth-joint contacts. In this study, three sets of models are established to explore the effects of stress state, fracture length and fracture orientation on the damage evolution in the rock specimen subject to a blast load. In the first set of models, we observe that when the horizontal stress σ_x is not equal to the vertical stress σ_y, the maximum slip of the pre-existing fracture is positively correlated with the differential stress, i.e. $\Delta\sigma = \sigma_x - \sigma_y$, which further leads to the generation of different numbers of secondary cracks. The second set of models shows that the number of secondary fractures grows as a quadratic power function with the increased length of the pre-existing fracture. Furthermore, extensive tensile stress regions emerge around the tips of secondary fractures. The third set of models focuses on the sensitivity analysis of fracture orientation, showing that with the clockwise rotation of the pre-existing fracture from the vertical direction, the number of secondary fractures decreases significantly but they are still concentrated locally at the tips of the pre-existing fracture. The research findings of our paper have important implications for the assessment of excavation damaged zone properties around nuclear waste repositories built using the drilling and blasting method.

1. Introduction

Subject to long-term and complex geological processes, numerous fractures of different geometries are usually accommodated in rocks [1,2]. These fractures have significant influences on the mechanical behavior of rock masses [3]. For instance, in rock engineering practices that use blasting frequently, these pre-existing fractures may weaken the strength of the rock mass and affect the propagation of

blast waves. A better understanding of the effects of these natural fractures as well as their interactions with blast-induced waves is of central importance for the assessment of excavation damaged zones for nuclear waste disposal.

Due to the importance of these pre-existing fractures, pre-fractured samples have been extensively studied experimentally and numerically in the past. Heekwang Lee [4] conducted uniaxial compression tests on polymethyl methacrylate (PMMA) samples as well as Diastone and Hwangdeung granite specimens, and analyzed the influence of pre-existing fractures on new crack propagation. Zhang et al.[5] studied the cracking processes initating from a pre-existing fracture by using the Particle Flow Code (PFC), and their results show that first cracks typically initiated from the regions of tensile stress concentration, which were partially released after the crack propagation. Yang et al.[6] conducted loading tests on sandstone samples with a single pre-existing fracture, and found that the length and angle of pre-existing rock have a key control on the strength and deformation behavior. Liu et al. [7] conducted a series of hydraulic fracturing tests to study the influence of prefabricated fractures with different inclination angles on the crack propagation in black shale. Combining the theory of maximum circumferential tensile stress and anisotropic analysis of stress field at the fracture tip, the initiation angle and equivalent stress intensity factor of the crack were obtained, and it was observed that with the increase of the fracture angle, both the fracturingmode and strength of the rock specimen changed.

However, the aforementioned studies have only focused on quasi-static loading conditions. Due to the transient nature of dynamic loading, crack propagation behaviour may become much more complex for rock under blast loading [8]. Research works have also been conducted to study explosion-induced wave propagation in rock masses via site monitoring and numerical simulations. Many constitutive models have been developed to quantify the response of rocks under extreme pressures and high strain rates, including the Johnson–Holmquist model [9], the Holmquist-Johnson-Cook model [10], the Talyor-Chen-Kuszmaul model [11] and Johnson-Holmquist-Rock model [12]. Rabczuk et al. [15] extended the cracking-particle method to deal with large deformation problems such as impact and blasting. Cho et al. [13] proposed a dynamic fracture process analysis to study the influence of waveform on the fracture propagation in rock; the results show that crack propagation depends not only on the peak value but also on the rise time of the applied pressure. Yang et al. [14] used a fully coupled fluid-solid interaction model to analyse blast-induced fracturing and fragmentation processes in fractured rocks. It is found that the in-situ stress also considerably affects the tensile damage region and fracture propagation behaviour of fractured rocks [15,16].

Although the above studies have considerably improved the understanding of the roles of pre-existing fractures, confining pressures and blasting loads in rock damage, the combined effects of in-situ stress state and pre-existing fracture on rocks subjected to dynamic loads have still been poorly understood so far. In this paper, we focus on the two-dimensional (2D) fractured rock subject to blasting-induced wave propagation and vibration. We explore three important parameters, i.e. in-situ stress state, fracture length and fracture orientation. The rest of the paper is organised as follows. Section 2 describes the numerical simulation results. The model setup including model design, boundary conditions and simulation procedures are described in Section 3. In Section 4, three sets of models are subjected to blast loads, and their geomechanical responses including fracture sliding and crack growth are investigated. Finally, a brief discussion is presented, after which conclusions are drawn.

2. DEM method and contact models

In this study, numerical simulation is performed using the particle flow code (PFC), which is capable of capturing fracture deformation and propagation in rocks under dynamic loads. At the beginning of the simulation, an intact rock is discretised into a large number of particles, while two types of contact models, i.e. the contact bond model (CBM) and the parallel bond model (PBM), are available for mimicking the interaction among these particles. The PBM model is more suitable for our study as it can capture the behavior of granite against bending moments, and is thus adopted in the rest of the paper.

In the PBM model, the tensile strength $\overline{\sigma}^{max}$ and shear strength $\overline{\tau}^{max}$ between neighbouring particles are given by

$$\overline{\sigma}^{max} = \frac{-\overline{F}^n}{A} + \frac{|\overline{M}^s|\overline{R}}{I_p} \tag{1}$$

$$\overline{\tau}^{max} = \frac{|\overline{F}^s|}{A} + \frac{|\overline{M}^n|\overline{R}}{J} \tag{2}$$

where $\overline{F}^n$ and $\overline{F}^s$ are the normal- and shear-directed force exerted by the contact, A and I_p are the area and moment of inertia of the contact cross-section, $\overline{\sigma}^{max}$ and $\overline{\tau}^{max}$ are the tensile and shear strength, respectively, and J is the polar moment of inertia.

The correlation between the force and the displacement at the contact is mainly determined by the normal stiffness $\overline{k}^n$ and the shear stiffness $\overline{k}^s$; the relation between normal stress and displacement can be described as:
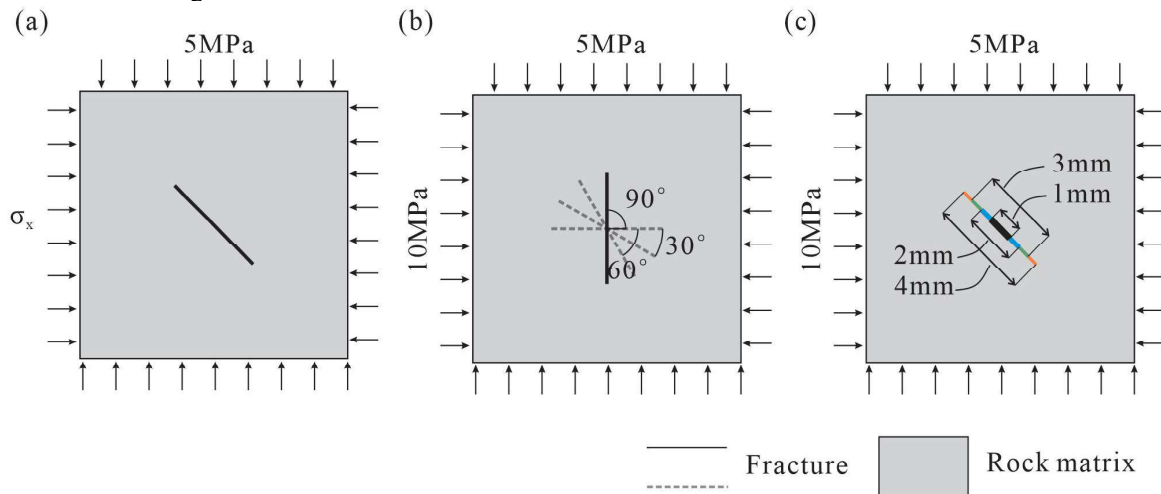
$$\sigma_n = -\overline{k}^n u_n \tag{3}$$

$$\tau_s = -\overline{k}^s u_s \tag{4}$$

where σ_n and τ_s are the normal and shear stress, respectively, while u_n and u_s are the normal and shear displacement, respectively. When the particles are under a force exceeding the tensile or shear strength, secondary cracks would initiate.
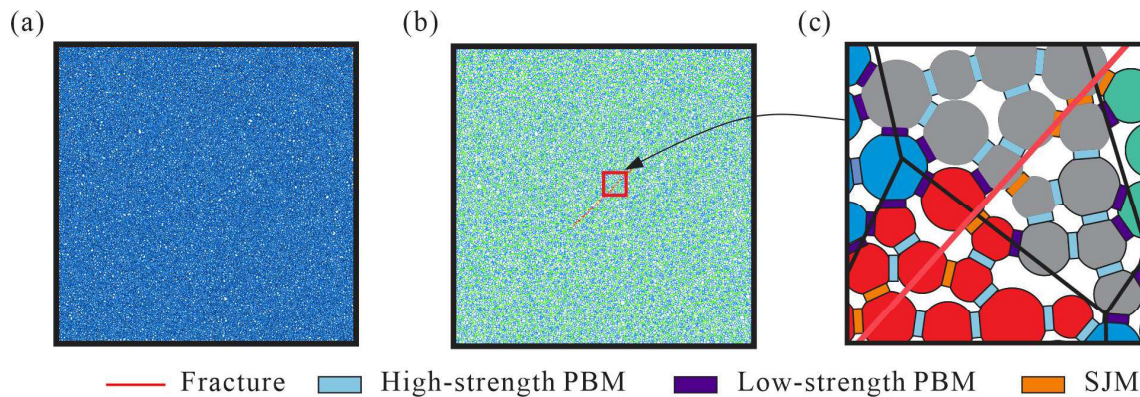
3. Model setup

3.1. Model design

Figure 1. Schematic illustrating the three variables we are considering: (a) differential stress, (b) fracture orientation, and (c) fracture length.

In this study, we generate 3 sets of particle-based models in a squared domain of size $L = 0.1$ m, aiming to explore the influences of differential stress, fracture length and fracture orientation on the damage evolution in the rock specimen subject to a blast load (Fig. 1). In the first set of models, three stress ratios are considered (i.e. $\sigma_x/\sigma_y = 1,2,3,4$); in the second and third sets of numerical experiments, four different fracture angles (i.e. 0° , 30° , 60° , 90°) and four different fracture lengths (i.e $L = 1,2,3,4mm$) are considered, respectively. The fractures in all these simulationsare represented by the smooth joint contact model (SJM).

Figure 2. Grain-Based model setup: (a) particle composition of the model, (b) model structure, and (c) the contact model on different structures.

As shown in Figure 2a, a square (100 mm × 100 mm) domain is created and more than 24000 particles (0.2-0.4mm) are generated. To capture realistic rock strength ratio (i.e. the ratio of uniaxial compressive strength to tensile strength), nonlinear failure envelope, and micro-crack evolution, the grain-based model (GBM) through an assembly of polygonal elements is used. In this study, the GBM is established based on the characterisation of the real grain structure of Beishan granite (Figure 2b). The contact strength within the unit is several times greater than that between the unit, even though all these contacts are based on the parallel bond model (Figure 2c).
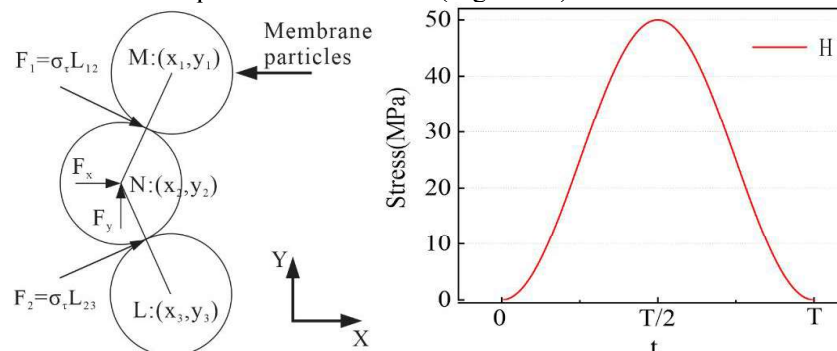
Figure 3. (a) Confining pressure applied to the membrane particles boundary. (b) Pressure-time curves for the blast wave.

Additionally, this paper proposes an approach to simulate the deep buried infinite bodies based on the flexible membrane. The functions for this boundary are described as follows:

The first function of the boundary is to apply confining pressure while allowing the model to deform freely. A two-dimensional schematic (Figure 3a) is provided to illustrate this method. F_1 and F_2 represent the equivalent force on the membrane segment, which renders the required confining pressure σ_r on the sample. F_x and F_y represent the force components applied onto the particle in the x and y direction, respectively, both of which are calculated based on a force balance relationship [17]:

$$F_x = 0.5(y_1 - y_3)\sigma_r \tag{5}$$
$$F_y = 0.5(x_1 - x_3)\sigma_r \tag{6}$$

where (x_1,y_1) and (x_3,y_3) are the coordinates of particles M and L, and σ_r is the required confining pressure.

When the blasting wave strikes the model boundary, it would be reflected backwardand may have a significant influence on the simulation results. To overcome this issue, we apply an reaction force based on the relationship between particle velocity and boundary forces, such that the flexible boundary absorbs the energy of blasting waves as expected. This reaction force is calculated as:

$$F = \begin{cases} -2\xi R\rho C_p \dot{u}_n \\ -2\eta R\rho C_s \dot{u}_s \end{cases} \tag{7}$$

where ξ and η are the correction coefficients of compressional and transverse waves, respectively; C_p and C_s are the longitudinal and transverse wave velocities, respectively; $\dot{u}_n$ and $\dot{u}_s$ are the normal and tangential motion velocities of particles, respectively.

Numerical results obtained by some researchers indicated that modelling only the stress wave propagation may give reasonable prediction of rock mass response to blasting load [13,18–21]. Thus, blasting damage to rock mass due to the pressure of the compressible gases is not considered in this investigation. The flexible membrane boundary on the left side possesses the capability of applying blasting waves. The pressure-time histories used for the numerical simulation are as shown in Figure 3b and given as:

$$H = 0.5(1 - \cos 2\pi f\, t) \tag{8}$$

where H is the blasting load, f is the frequency of the incident wave, and t is the time.

3.2. Parameter calibration

To reproduce realistically the mechanical behavior of the granite, it's necessary to calibrate the micro-mechanical parameters by comparing the numerical model against laboratory tests. The geometric dimensions of the calibration models are consistent with the laboratory specimen, i.e. 50 mm in width and 100 mm in height. The appropriate micro-parameters were determined via a systematic process of 'trial and error'. Finally, the calibrated results of the Beishan granite are shown in Table 1.

Table 1. Properties of Beishan granites in laboratory and numerical simulation

Property	Beishan granite (laboratory)	Beishan granite (numerical)	Error
Uniaxial compression strength(MPa)	120.0	114.8	4.33%
Tensile strength (MPa)	12.5	13.0	-4.00%
Young's modulus (GPa)	53.0	51.8	2.26%
Poisson's ratio	0.240	0.244	-1.67%

## 4. Result

4.1. Effect of stress ratio
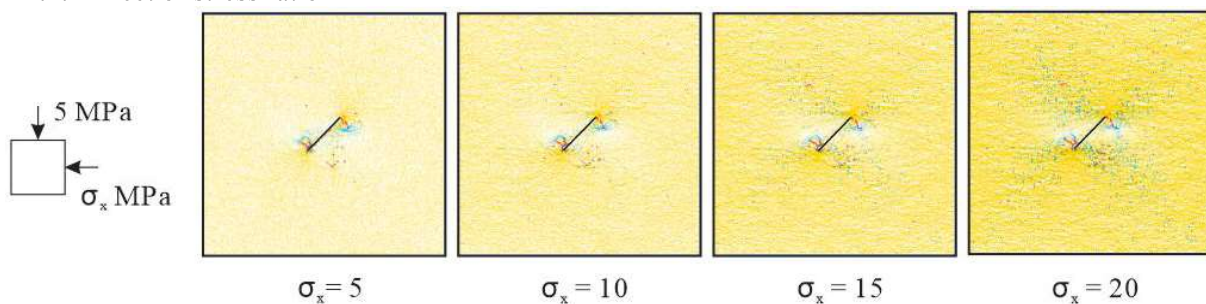
Figure 4. Force chains of the models affected by different differential stresses.

The distribution of secondary cracks and stress in the model subject to four different in-situ stress ratio cases ($\sigma_x/\sigma_y = 1\ to\ 4$) are shown in Figure 4. Secondary cracks mainly initiate from the tips of the fracture and tend to have an initial propagating direction perpendicular to the fracture. An increase in both the number of new cracks and the area of tensile regions is observed with the increased stress ratio. In particular, it can be seen that the shape of the tension region in the model under a low stress ratio is different from that in the model under a high stress ratio. In the case where $\sigma_x/\sigma_y \leq 2$, the

tensile regions concentrates at the tips of the pre-existing fracture; in the case of $\sigma_x/\sigma_y \geq 3$, the tensile stress is more spatially distributed into the four lobes , showing a shape of four-leaf clover.

4.2. Effect of fracture orientation
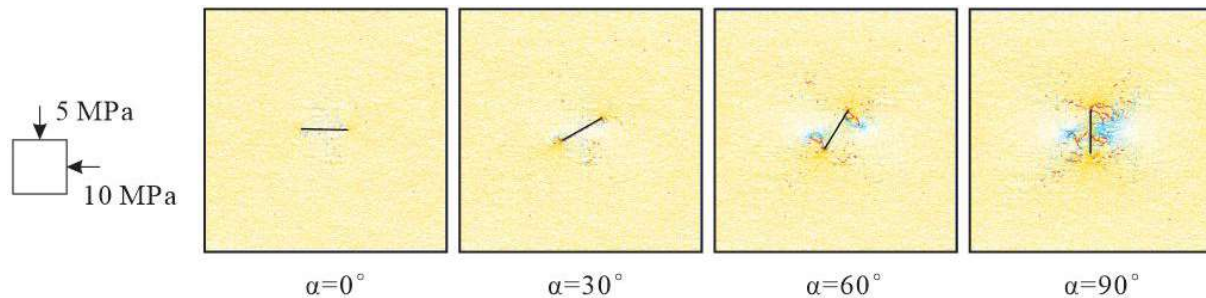
Figure 5. Force chains of models with different fracture angles.

The influence of the blast-induced stress wave on crack propagationis also related to the fracture orientation. Figure 5 presents a series of plots of the models with different fracture orientations. In the case of $\alpha = 0°$, there are almost no secondary cracks or tension regions in the model, indicating that the pre-existing fracture oriented parallel to the blast wave propagating direction has little effect on the mechanical properties of granite. As α increases, significant secondary cracks emerege, and the tension region is concentrated around these cracks as the result of stress release caused by secondary cracks. When the angle between the wave direction the primary fracture is $60°$, secondary cracks developed from the tips of the pre-existing fracture, and the tension region exhibits evident regularity in the distribution, which are concentrated at the tips of secondary cracks. When the angle reached $90°$, the secondary cracks are no longer centered at the tips of the primary fracture and extend to both lateral spaces. In addition, as the fracture orientation α increases, the stress concentration at the fracture tips becomes more obvious. The simulation results show a good consistency with the research by Hao et.al [22].
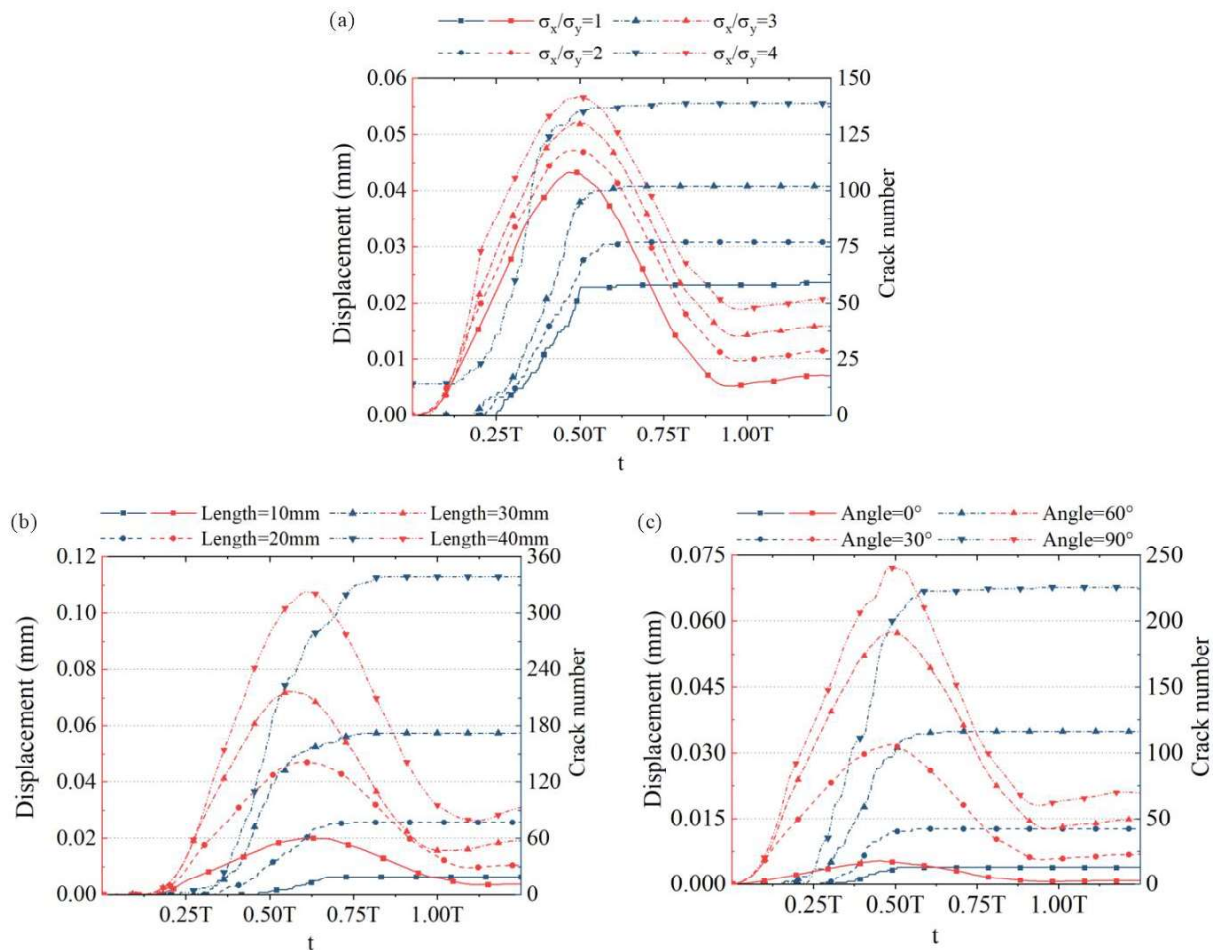
4.3. Effect of fracture length
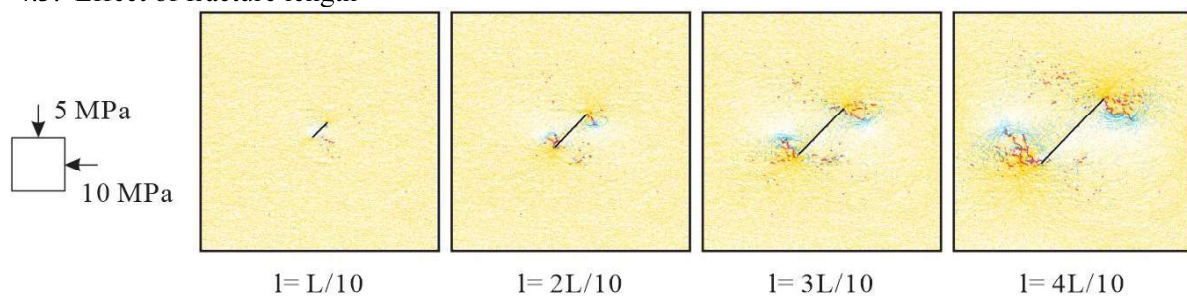
Figure 6. Force chains of models with different fracture lengths.

Figure 6 presents the simulation results for different fracture lengths ranging from $l/10$ to $4l/10$, while the in-situ stress is kept the same. It can be seen that the shorter fracture only has a minor effect on the propagation of cracks. By comparing the models in Figure 8, it's obvious that an increased fracture length causes the formation of more new cracks and larger tensile regions, but the pattern of cracks propagation and stress distribution is similar. The relationship between the fracture length and secondary cracks is further quantitatively analyzed in Figure7.

4.4. Variation of fracture displacement and crack number

Figure 7. Variation of fracture displacement and number of secondary cracks with time. (a) Differential stress variable group. (b) Fracture angle variable group. (c) Fracture length variable group.

The variation of fracture displacement and crack number with time is illustrated in Figure 7. By comparing Figure 7 with Figure 3b, it can be found from their similar wave shape that a strong correlation between fracture displacement and blasting wave. Furthermore, with the increase of fracture displacement, the number of cracks increases. After the displacement arrived at the maximum value, the number of new cracks reaches a plateau, implying that the crack extension would be dependent predominantly on the peak value and pre-peak stage of the blasting wave, regardless of the post-peak stage. Such a correlation between the blast wave and new cracks seems to hold for different scenarios of fracture lengths, stress states, and fracture orientations.
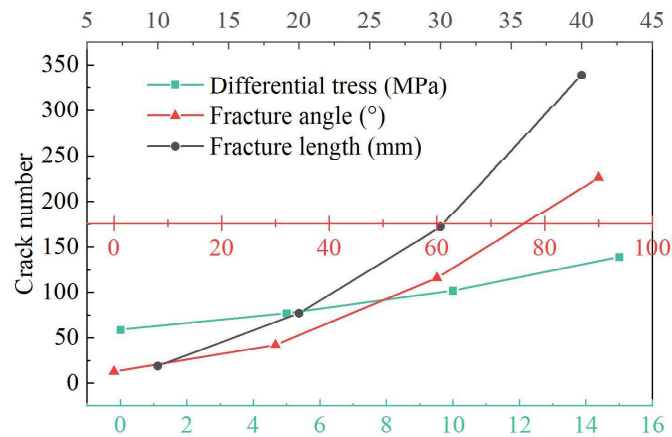
Figure 8. Statistics on the number of cracks

We further study the relationships between the values of different variables and the number of cracks (Figure 8). The increase of the three variables will lead to the increase of the number of secondary cracks.

5. Discussion

To explore the mechanism behind the phenomenon, we establish a local coordinate system with the axes of x and y parallel and perpendicular to the bottom edge of the model, respectively (Figure 9).
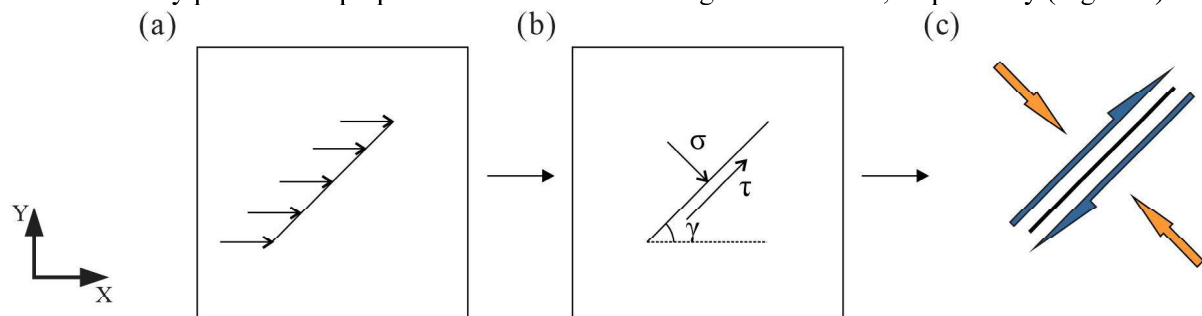

Figure 9. Analysis of the effect of blasting stress on pre-existing fracture

When the blasting wave is transmitted to the pre-existing fracture, we analyze the blast-induced stress exerted on the fracture plane. The force is made up of two parts: the normal stress σ perpendicular to the direction of the fracture and the shear stress τ parallel to the fracture (Figure 9b), which further leads to the displacement of the fracture (Figure 9c). Figure 10 displays the influence of fracture displacement in the noraml and tangential directions on the tensile stress pattern.
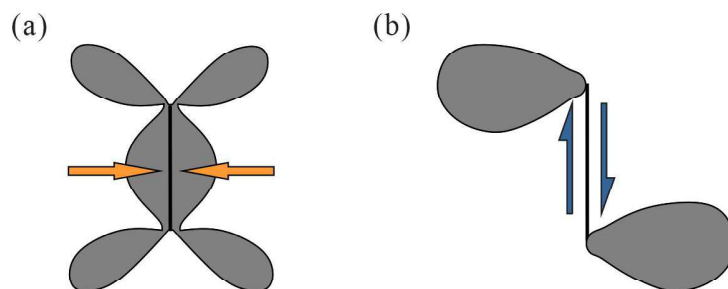
Figure 10. Stress disturbance caused by fracture displacement. (a) The displacement in the tangential direction. (b) The displacement in normal direction.
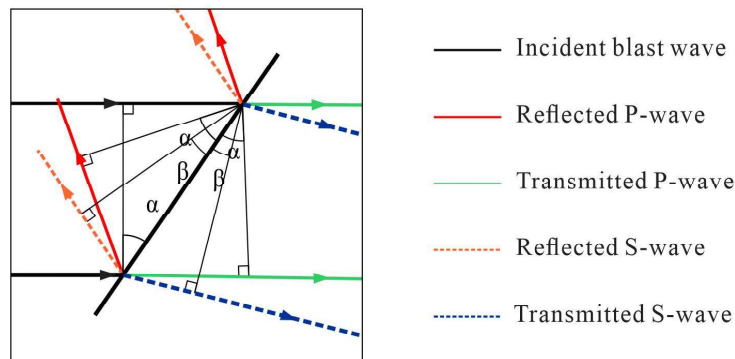
Figure 11. Reflection and transmission of burst wave on fracture surface.

As shown in figure 11, when a blast wave impinges on the fracture, both reflection and transmission take place [23]. According to the conservation of momentum on the wave fronts, the relation between the stresses on the two interfaces of the joint and the particle velocities is then established. the stresses on the left interface of the joint can be expressed as[24]:

$$\sigma_{wave} = \rho c_p \upsilon_{Ip} \cos 2\beta + \rho c_p \upsilon_{Rp} \cos 2\beta - \rho c_s \upsilon_{Rs} \sin 2\beta \qquad (9)$$

$$\tau_{wave} = \rho c_p \upsilon_{Ip} \sin 2\beta \tan \beta \cot \alpha - \rho c_p \upsilon_{Rp} \sin 2\beta \tan \beta \cot \alpha - \rho c_s \upsilon_{Rs} \cos 2\beta \qquad (10)$$

Considering the influence of in-situ stresses, σ and τ are given by:

$$\sigma = \sigma_{in-situ} + \sigma_{wave}$$
$$= \sigma_x \cos^2 \gamma + \sigma_y \sin^2 \gamma + \rho c_p \upsilon_{Ip} \cos 2\beta + \rho c_p \upsilon_{Rp} \cos 2\beta \qquad (11)$$
$$- \rho c_s \upsilon_{Rs} \sin 2\beta$$

$$\tau = \sigma = \sigma_{in-situ} + \sigma_{wave}$$
$$= \frac{1}{2}(\sigma_y - \sigma_x) \sin 2\gamma + \rho c_p \upsilon_{Ip} \sin 2\beta \tan \beta \cot \alpha \qquad (12)$$
$$- \rho c_p \upsilon_{Rp} \sin 2\beta \tan \beta \cot \alpha - \rho c_s \upsilon_{Rs} \cos 2\beta$$

where υ_{Ip} and υ_{Rp} are the particle velocities of the incident and reflected P-waves, respectively; υ_{Rs} is the particle velocities of the reflected S-waves; ρ is the density of the intact rock; c_p and c_s are the velocities of the P- and S-waves in the intact rock.

It can be seen that, under the condition of constant blast-induced stress and σ_y, an increase of σ_x leads to the increase of both σ and τ and then induces a larger fracture displacement, conststent with our simulation. In addition, under the condition that the fracture length increases while the stress remains constant, it is expected that the fracture will slip more.

6. Concluding remarks

In this paper, we conducted numerical simulations to investigate blast-induced crack propagation in rock specimens embedded with a pre-existing fracture. We used an absorption boundary condition around the models to simulate waves in an infinite medium. Our results illustrate that the orientation and length of the pre-existing fracture as well as the in-situ stress play important roles in the crack propagation. Specifically, we found that the differencial stress in the same direction as the blasting wave will strengthen the blasting effect, and the mechanism was explored theoretically. In addition, the fracture normal to the propagation direction of the blasting wave has a stronger response to the blasting wave, while the response decreases as the fracture orientation decreases.

References

[1]   Cao R hong, Cao P, Lin H, Pu C zhi and Ou K 2016 Mechanical Behavior of Brittle Rock-Like Specimens with Pre-existing Fissures Under Uniaxial Loading: Experimental Studies and Particle Mechanics Approach *Rock Mech. Rock Eng.* **49** 763–83

[2]   Wei M D, Dai F, Xu N W and Zhao T 2016 Stress intensity factors and fracture process zones of ISRM-suggested chevron notched specimens for mode I fracture toughness testing of rocks *Eng. Fract. Mech.* **168** 174–89

[3]   Jing L 2003 A review of techniques, advances and outstanding issues in numerical modelling for rock mechanics and rock engineering *Int. J. Rock Mech. Min. Sci.* **40** 283–353

[4]   Lee H and Jeon S 2011 An experimental and numerical study of fracture coalescence in pre-cracked specimens under uniaxial compression *Int. J. Solids Struct.* **48** 979–99

[5]   Zhang X P and Wong L N Y 2012 Cracking processes in rock-like material containing a single flaw under uniaxial compression: A numerical study based on parallel bonded-particle model approach *Rock Mech. Rock Eng.* **45** 711–37

[6]   Yang S Q and Jing H W 2011 Strength failure and crack coalescence behavior of brittle sandstone samples containing a single fissure under uniaxial compression *Int. J. Fract.* **168** 227–50

[7]   Liu D, Shi X, Zhang X, Wang B, Tang T and Han W 2018 Hydraulic fracturing test with prefabricated crack on anisotropic shale: Laboratory testing and numerical simulation *J. Pet. Sci. Eng.* **168** 409–18

[8]   Wu Z and Wong L N Y 2014 Investigating the effects of micro-defects on the dynamic properties of rock using Numerical Manifold method *Constr. Build. Mater.* **72** 72–82

[9]   Johnson G R and Holmquist T J 1994 An improved computational constitutive model for brittle materials **981** 981–4

[10]   Holmquist T J and Johnson G R 1993 A computational constitutive model for glass subjected to large strains, high strain rates and high pressures *J. Appl. Mech. Trans. ASME* **78** 1–10

[11]   Taylor L M, Chen E P and Kuszmaul J S 1986 Microcrack-induced damage accumulation in brittle rock under dynamic loading *Comput. Methods Appl. Mech. Eng.* **55** 301–20

[12]   Xie L X, Yang S Q, Gu J C, Zhang Q B, Lu W B, Jing H W and Wang Z L 2019 JHR constitutive model for rock under dynamic loads *Comput. Geotech.* **108** 161–72

[13]   Cho S H and Kaneko K 2004 Influence of the applied pressure waveform on the dynamic fracture processes in rock *Int. J. Rock Mech. Min. Sci.* **41** 771–84

[14]   Yang P, Lei Q, Xiang J, Latham J P and Pain C 2020 Numerical simulation of blasting in confined fractured rocks using an immersed-body fluid-solid interaction model *Tunn. Undergr. Sp. Technol.* **98** 103352

[15]   Xie L X, Lu W B, Zhang Q B, Jiang Q H, Wang G H and Zhao J 2016 Damage evolution mechanisms of rock in deep tunnels induced by cut blasting *Tunn. Undergr. Sp. Technol.* **58** 257–70

[16]   Wang Z L and Konietzky H 2009 Modelling of blast-induced fractures in jointed rock masses *Eng. Fract. Mech.* **76** 1945–55

[17]   Wang Y H and Leung S C 2008 A particulate-scale investigation of cemented sand behavior *Can. Geotech. J.* **45** 29–44

[18]   Donzé F V., Bouchez J and Magnier S A 1997 Modeling fractures in rock blasting *Int. J. Rock Mech. Min. Sci.* **34** 1153–63

[19]   Hao H, Wu C and Zhou Y 2002 Numerical analysis of blast-induced stress waves in a rock mass with anisotropic continuum damage models Part 1: Equivalent material property approach *Rock Mech. Rock Eng.* **35** 79–94

[20]   Ma G W and An X M 2008 Numerical simulation of blasting-induced rock fractures *Int. J. Rock Mech. Min. Sci.* **45** 966–75

[21]   Shin J H, Moon H G and Chae S E 2011 Effect of blast-induced vibration on existing tunnels in soft rocks *Tunn. Undergr. Sp. Technol.* **26** 51–61

[22]   Hao H, Wu Y, Ma G and Zhou Y 2001 Characteristics of surface ground motions induced by blast in jointed rock mass *Soil Dyn. Earthq. Eng.* **21** 85–98

[23]   Kolsky H 1953 Natur e 707 3651

[24]   Li J and Ma G 2010 Analysis of blast wave interaction with a rock joint *Rock Mech. Rock Eng.*
         43 777–87